ADVANCED FUNCTIONAL MATERIALS
www.afm-journal.de

Photoswitchable Conductive Metal–Organic Frameworks

*Yidong Liu, Mersad Mostaghimi, Abhinav Chandresh, Saibal Jana, Wolfgang Wenzel, and Lars Heinke**

Advanced materials with physical properties such as electric conductivity that can be dynamically controlled by remote signals will enable new cutting-edge applications. To date, while many materials with either photoswitchable conduction properties or high conductivities have been presented, the combination of both properties remains a challenge. Here, a series of conductive metal–organic framework (MOF) thin films is presented where the conductivity is reversibly remote controlled by light. The structures of the MOFs are Cu_3(2,3,6,7,10,11-hexahydroxytriphenylene)$_2$ (Cu_3(HHTP)$_2$) with different photochromic molecules of type azobenzene (AB), diarylethene (DAE), spiropyran (SP) and hexaarylbiimidazole (HABI) derivatives embedded in the MOF pores. By photoisomerizations of the guest molecules, induced by UV light and reversed by visible light irradiation or thermal relaxation, the conduction properties of the photoswitch@Cu_3(HHTP)$_2$ films are reversibly modulated by up to 15%. These changes of the electrical conductivity can be understood by calculating the density of states (DOS) near the Fermi level, showing that the DOS decreases upon embedment of the guest molecules and as a result of their isomerization. Moreover, the application of such photoswitch@Cu_3(HHTP)$_2$ films as photoprogrammable gas sensors is demonstrated. With the introduction of photoswitchable conductive hybrid material, this study contributes to the extension of smart materials for innovative applications.

1. Introduction

Smart materials allow the adaptation and modification of their properties by external stimuli. Especially light is a highly attractive stimulus that offers many advantages such as a fast, dosable, and practical signal allowing for remote control over long distances.[1–3] Light-responsive materials are often derived from photoactive organic molecules.[4,5] Such photoresponsive components enable the design of materials with various tailored responses, including changes in color, shape or conductivity, upon exposure to specific light conditions.[6,7] Commonly used photochromic molecules, capable of bistable states under light irradiation of different wavelengths, play a pivotal role in conferring stimulus-responsive properties to materials. Examples of common photochromic molecules are azobenzene,[5] diarylethene,[4] and spiropyran,[8] which undergo reversible isomerization under UV and visible light irradiation (or thermal relaxation) between two (meta-) stable forms. The light-controlled regulation of electrical properties is highly attractive which enables photoresponsive materials to be used in various fields of advanced electronic applications. To date, various classes of materials combined with different photochromic materials were produced, see Table S1 (Supporting Information). For example, diarylethene-based polymers with a conductivity of $\approx 1.2 \times 10^{-10}$ S m^{-1} were made where the conductivity can be modulated by light by factor 2.3[9] or azobenzene-based polymers with carbon nanotubes with a conductivity of $\approx 10^{-3}$ S m^{-1} and an On-Off-ratio of 1.3.[10] Despite the effort, these materials possess rather low conductivities compared to common electronic conductors (Table S2, Supporting Information), which have typically conductivities of much larger than 1 S m^{-1}. To date, materials that combine high conductivity and photo-responsive properties have not yet been presented.

Metal–organic frameworks (MOFs) represent a distinct class of porous crystalline materials characterized by the assembly of metal nodes/clusters and organic linkers.[11,12] Over the past few decades, the field has witnessed rapid advancements owing to the deliberate design and synthesis of innovative ligands, coupled with the manipulation of self-assembly and interfacial structures. This concerted effort has resulted in the development of MOFs exhibiting remarkable electronic and protonic conduction

Y. Liu, L. Heinke
Institute of Functional Interfaces (IFG)
Karlsruhe Institute of Technology (KIT)
Hermann-von-Helmholtz-Platz 1,
76344 Eggenstein-Leopoldshafen, Germany
E-mail: lars.heinke@fu-berlin.de
M. Mostaghimi, S. Jana, W. Wenzel
Institute of Nanotechnology (INT)
Karlsruhe Institute of Technology (KIT)
Hermann-von-Helmholtz-Platz 1,
76344 Eggenstein-Leopoldshafen, Germany
A. Chandresh, L. Heinke
Physical Chemistry
Institute of Chemistry and Biochemistry
Freie Universität Berlin
Arnimallee 22, 14195 Berlin, Germany

The ORCID identification number(s) for the author(s) of this article can be found under https://doi.org/10.1002/adfm.202423539

DOI: 10.1002/adfm.202423539

properties.[13] The electrical properties of these MOF materials have promoted their application in diverse fields such as sensors, supercapacitors, electronics, and spintronics.[14–16] Particularly, planar multidentate ligands like triphenylene derivatives (e.g., hexahydroxytriphenylene (HHTP) and hexaiminotriphenylene) have been instrumental in forming 2D MOFs with exceptional electrical characteristics upon coordination with metals such as Fe, Co, Ni or Cu.[17–20] This high degree of π-electron delocalization contributes to outstanding electrical conductivity, exemplified by $Cu_3(HHTP)_2$ thin film. For $Cu_3(HHTP)_2$ materials made with different methods, the conductivities determined with different methods are approximately in the range of 0.2 S m^{-1} to 20 S m^{-1}, Table S3 (Supporting Information). On the other hand, stimulus-responsive MOF materials have also been a focus of MOF research, showcasing potential applications in sensors, memories, and smart devices.[21–24] To date, various photoresponsive molecules like azobenzene,[25–27] diarylethene[21,28,29] or spiropyran[21,30–32] but also less common photoswitchable molecules like hexaarylbiimidazole[33] have been incorporated in the MOF material, either through embedment in the pores or by incorporation in the MOF structure (either in the backbone or as side group). In our prior study, spiropyran was embedded in MOFs of the type UiO-67, leading to a reversible photomodulation of the conductivity by one order of magnitude and conductivity values in the order of 10^{-8} S m^{-1}.[34] Although theoretical calculations show that the On-Off-switching ratio can be further enhanced to more than two orders of magnitude,[35] this approach seems not suited to realize highly conducting materials with photo-modulable conductivity.

In this study, a conductive material with a conductivity that can be controlled by light is presented. The material is based on highly conductive MOFs of type $Cu_3(HHTP)_2$, made in a layer-by-layer fashion referred to as surface-mounted MOFs (SURMOFs).[36] The controlled growth of $Cu_3(HHTP)_2$-SURMOFs ensures a highly anisotropic structure, with the MOF-planes parallel to the substrate and the pores perpendicular to the substrate.[37] By incorporating photochromic molecules, namely azobenzene (AB), pyridinyl-diarylethene (DAE), nitro-spiropyran (SP) or ortho-chloro-hexaarylbiimidazole (HABI), into the pores of the $Cu_3(HHTP)_2$ SURMOF thin film, hybrid photochromic SURMOF films, namely AB@$Cu_3(HHTP)_2$, DAE@$Cu_3(HHTP)_2$, SP@$Cu_3(HHTP)_2$ and HABI@$Cu_3(HHTP)_2$, **Figure 1**, were prepared. The conductivity of these films was controlled through UV/vis irradiation. The reversible photoisomerization of the embedded photochromic molecules within the $Cu_3(HHTP)_2$ pores was investigated using UV-vis spectroscopy. Subsequent direct current (DC) conductivity measurements revealed bistable electric conduction properties in these hybrid SURMOF films. The conductivities of these films demonstrate reversible alterations under UV/visible irradiation or thermal relaxation. Notably, HABI@$Cu_3(HHTP)_2$ exhibits a conductivity of ≈4 S m^{-1} and a remarkable conductivity change of up to 15.2 % through UV irradiation and thermal relaxation. This occurs because the introduction and isomerization of guest molecules affect the DOS around the Fermi level in the MOF, thereby (indirectly) altering the electrical conductivity of the framework. Furthermore, we demonstrate that the HABI@$Cu_3(HHTP)_2$ film is still porous and it can be used as photoresponsive electric gas sensor for different molecules (like water, ethanol, toluene, and 1-propanol). This groundbreaking achievement represents the development of photoswitchable conductive SURMOF materials through the incorporation of photochromic molecules.

2. Results and Discussion

The fabrication of the $Cu_3(HHTP)_2$ SURMOF films was carried out in a layer-by-layer fashion.[36] A dipping robot[38] was used which exposes the substrate successively to the solutions containing the SURMOF components, i.e., the Cu-metal nodes and the HHTP linker molecules. The substrates for the SURMOF were quartz glass plates for UV-vis spectroscopy and interdigitated gold electrodes on quartz glass sheets (IDE) for electrical measurements. The photochromic molecules were introduced into the SURMOF film by immersing the sample in ethanolic solutions of AB, DAE, SP, and HABI.

Figure 2a shows the X-ray diffraction (XRD) patterns of the synthesized $Cu_3(HHTP)_2$ SURMOF film, revealing a crystalline structure consistent with the targeted structure. Notably, the out-of-plane (oop) XRD displays only the (001) peak, indicating the oriented growth of the MOF film. This high level of crystalline orientation is further indicated by the in-plane (ip) XRD patterns, which exclusively feature reflections perpendicular to the [001] direction. These findings confirm the crystalline and highly oriented nature of the $Cu_3(HHTP)_2$ SURMOF, highlighting the formation of layers parallel to the substrate through the alignment of copper atoms and HHTP linker molecules. Upon loading the $Cu_3(HHTP)_2$ SURMOF with photochromic molecules, a change in the intensity ratio of the in-plane XRD reflections was observed. For HABI, the ratio of the intensities for the (100) peak compared to the (200) peak decreased from 6.5 to 3.2. Similar changes were found in AB@$Cu_3(HHTP)_2$, DAE@$Cu_3(HHTP)_2$ and SP@$Cu_3(HHTP)_2$, Figure S1 (Supporting Information), showing a change in the XRD form factor and indicating successful loading of the guest molecules in the MOF pores.

The scanning electron microscope (SEM) images of the samples are shown in Figure S2 (Supporting Information).They demonstrate that the $Cu_3(HHTP)_2$ SURMOF films possess a dense and continuous morphology. From cross-sectional SEM images, a film thickness of ≈0.5 µm was estimated. For the quantitative analysis of the amounts of photochromic molecules embedded in the pores, energy-dispersive X-ray (EDX) spectroscopy was employed, Figure S3 (Supporting Information). We use the fact that copper is present only in the SURMOF host while nitrogen and sulfur are present only in the photoswitchable guests. Based on the fact that each crystallographic unit cell of $Cu_3(HHTP)_2$ features three copper atoms per one pore, we calculated the pore loadings from the atomic EDX ratios. As a result, we found that each unit cell of $Cu_3(HHTP)_2$, with a cylindrical pore of 2.0 nm in diameter and a height of 0.3 nm, is loaded with 0.35, 0.56. 0.38 and 0.23 photoswitches of type AB, DAE, SP, and HABI, respectively, on average. The MOF pores with the respective average amount of photoswitches are shown in the supporting information, Figure S3r–u (Supporting Information), visualizing that the pore packing is rather high. Moreover, the EDX-elemental-distribution maps, Figure S3 (Supporting Information), show that the photoswitchable molecules

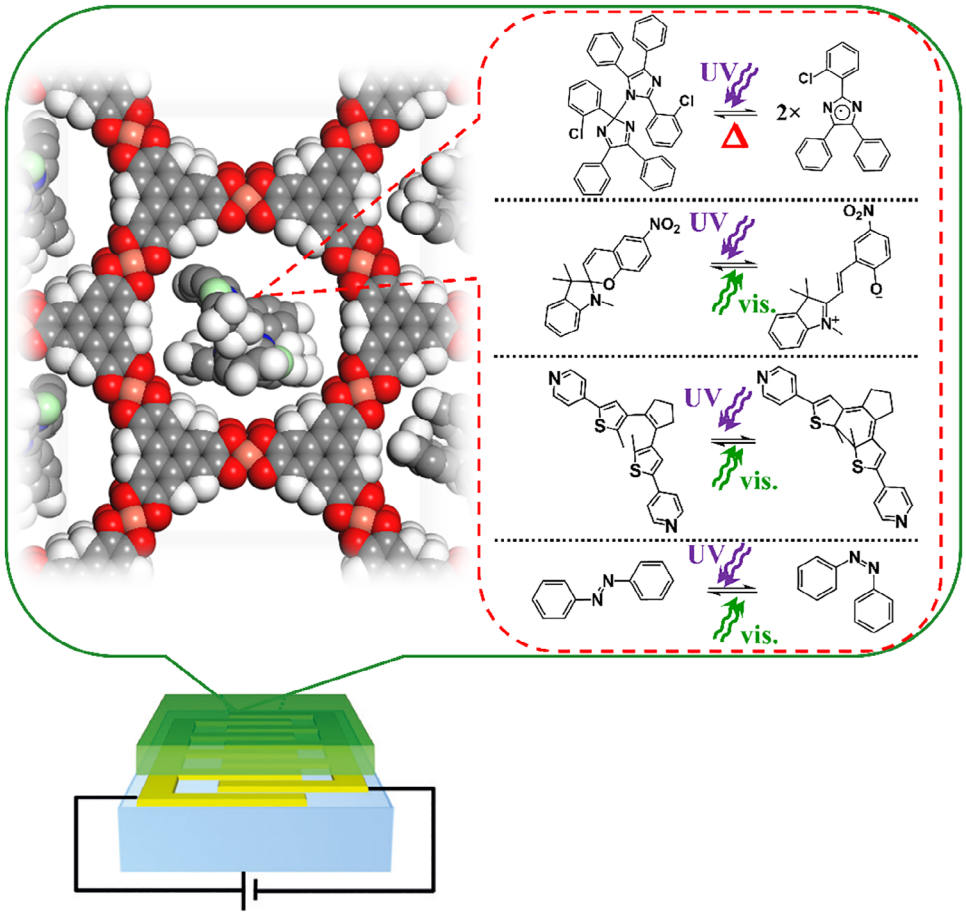

Figure 1. Sketch of 2D SURMOF $Cu_3(HHTP)_2$ with one embedded photochromic HABI molecule in the pores. The color code of the atoms is C gray, H white, O red, N blue, Cl green, Cu orange. In the study, instead of HABI, SP, DAE, and AB were also embedded in the pores. Light-induced reactions of these molecules are shown on the right-hand side. There, the thermodynamically stable state is shown on the left (dimer-HABI, SP, open-DAE, and *trans*-AB, top to bottom), the meta-stable state upon excitation with UV light is shown on the right-hand side (radical-HABI, MC, closed-DAE and *cis*-AB). A SURMOF film on interdigitated gold electrodes (to measure the DC conduction) is sketched below.

are homogeneously distributed in the SURMOF films. (Since a closed packing or even crystalline packing of the photoswitches would sterically hinder their isomerization,[39–41] the observed photoisomerization, see below, suggests that the photoswitches are dispersed in the pores.)

The photoisomerization in the photoswitch@$Cu_3(HHTP)_2$ samples was investigated using UV-vis spectroscopy, Figure 2b–e). For comparison, the spectra of the ethanolic AB, DAE, SP, and HABI solution (i.e., without MOF) are shown in Figure S4 (Supporting Information). For all four photoswitch@SURMOF samples, it was found that the light-induced spectral changes are very similar to the light-induced spectral changes of the respective molecule in solution. This indicates that the light-induced isomerizations of the photoswitches in the MOF pores are similar to the light-induced isomerizations in solution. This is similar to previous photoswitch@SURMOF studies.[34,42,43] For example, in the spectrum of the AB@$Cu_3(HHTP)_2$ sample (Figure 2b), the absorption intensity at 320 nm decreases upon UV light irradiation of 365 nm, while the absorption intensity at 450 nm increases. Subsequent irradiation with 455 nm light results in a restoration of the initial spectrum, indicating the *trans*-to-*cis* photoisomerization of the AB molecule by UV-light and *cis*-to-*trans* by blue light.[42] For DAE@$Cu_3(HHTP)_2$ (Figure 2c), the absorption intensities at 386 nm and 580 nm increase upon exposure to UV light of 365 nm and decrease again upon green light of 530 nm. This indicates the ring-opening and ring-closing of the DAE molecule by green and UV light, respectively. Similarly, reversible changes in the absorption band at 550 nm are observed for SP@$Cu_3(HHTP)_2$ (Figure 2d) under irradiation at 365 nm and 530 nm, indicating the SP-to-MC (merocyanine) isomerization of the SP molecule.[34] In Figure 2e, the absorption band changes of HABI@$Cu_3(HHTP)_2$ are presented. The UV-vis spectrum exhibits small changes of the absorption bands at 303 and 443 nm. This spectral evolution signifies the transformation of HABI embedded in the MOF pores from the dimer state to the radical state upon UV irradiation and vice versa by thermal relaxation at elevated temperatures.[33,44] All of these spectral changes are reversible and repeatable, indicating the reversible and repeatable isomerization of the photoswitches in the MOF pores. As a result, the spectroscopic analysis of the UV-vis absorption spectra shows that light-induced isomerizations of

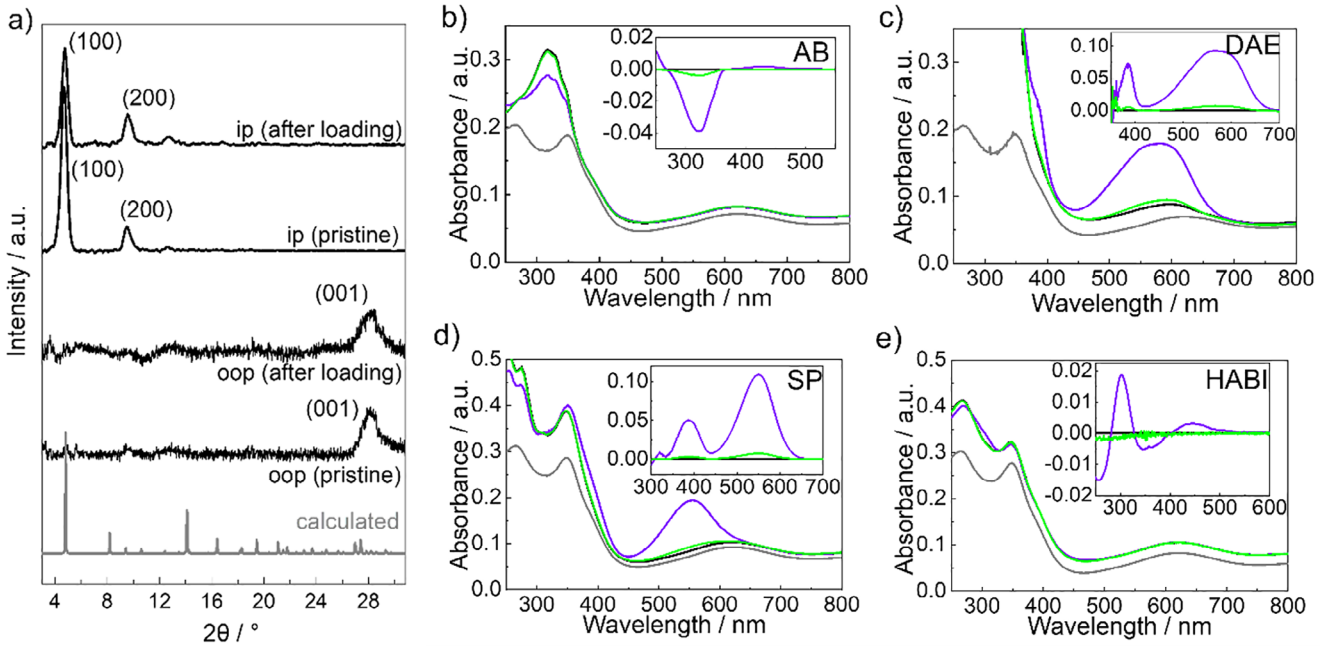

Figure 2. a) In-plane (ip) and out-of-plane (oop) XRD data of the HABI@$Cu_3(HHTP)_2$ sample, before and after the guest loading, see labels. The data are compared with the calculated XRD for a powder sample (grey). The X-ray wavelength is 0.154 nm. The experimentally observed diffraction peaks are labeled. b)-e) UV-vis spectra of the photoswitch@$Cu_3(HHTP)_2$-SURMOF samples measured in transmission mode for the different photoswitchable guest molecules b) AB, c) DAE, d) SP and e) HABI. The color code is: grey for the spectra of the empty $Cu_3(HHTP)_2$ SURMOF samples; black for the samples after the photoswitch loadings; violet after UV-irradiation and green after switching back (via visible-light irradiation or thermal relaxation). The insets show the differential spectra with the pristine loaded-SURMOF spectra as references.

the photoswitches in the $Cu_3(HHTP)_2$ MOF pores are similar to the isomerizations in solution. In previous studies, the yields of the photoisomerization of the photoswitches embedded in the pores of a MOF under the same (or very similar) experimental conditions were determined to be 65% for AB,[42] 70% for SP[34] and 84% for HABI,[43] respectively. For DAE, the yield of the photoisomerization was determined for the DAE molecule incorporated in the MOF structure where the photoisomerization yield is 60%.[28] It was found that the isomerization is rather fast and the equilibrium is reached within a few minutes or faster, thus, the used irradiation time is sufficient to reach the equilibrium (final) photoisomerization yield.

The electrical conduction properties of the photoswitch@$Cu_3(HHTP)_2$ films were investigated by 2-probe DC measurements. For precise and reproducible conductivity measurements with the identical sample, the samples were prepared on substrates with interdigitated gold electrodes (IDEs). The current at a constant DC voltage of +1 V was recorded and the conductivity was calculated based on the film thickness and IDE geometry. In order to assess the impact of the loading with the photochromic molecules on the electric conductivity of the $Cu_3(HHTP)_2$ SURMOF film, the changes of electrical conductivity of the same sample before and after the loading/unloading process were explored, **Figure 3a**. It shows that the initial electric conductivity of the pure $Cu_3(HHTP)_2$ SURMOF film was 4.13 S m^{-1}, which is in agreement with the conductivity values found by other groups (see Table S3, Supporting Information).[19,45] Upon loading with HABI, the conductivity of the SURMOF film decreases to 3.75 S m^{-1}. Unloading HABI by immersing the sample in ethanol restores the initial conductivity. The loading and unloading of SP, AB, and DAE in the SURMOF shows a similar reversible decrease of conductivity. While the loading of all four photoswitches results in a decrease of the conductivity which is fully reversible by unloading the photoswitch again, there are small quantitative differences between the molecules. The relative reduction of the conductivity is 9.2%, 5.6%, 5.3%, and 4.9% for HABI, SP, AB, and DAE, respectively. This means the loading-induced conduction changes depend strongly on the molecule.

In the next step, the impact of the photoswitching is explored. This means we focus on the changes of the conductivity as a response to the light-induced isomerization of the photoswitch in the $Cu_3(HHTP)_2$ film. The current versus time curves of the DAE@$Cu_3(HHTP)_2$ film and of the HABI@$Cu_3(HHTP)_2$ film over three consecutive switching cycles with UV-light and relaxation are depicted in Figure 3b,c, respectively. For HABI@$Cu_3(HHTP)_2$, it shows that upon UV-light-induced dimer-to-radical isomerization of HABI, the current drops from ≈24.5 to 21 mA. Upon thermal radical-to-dimer isomerization of HABI, the initial current (and conductivity) was restored. That process is reversible and repeatable. For DAE@$Cu_3(HHTP)_2$, the reversible ring-opening/-closing of DAE results in a reversible switching of the current between 24.1–25.6 mA. For the other photoswitches (AB and SP), similar light-responsive switching behavior was observed, Figure S5 (Supporting Information). For example, for AB@$Cu_3(HHTP)_2$ (Figure S5a, Supporting Information), the reversible *trans-cis* AB photoswitching with UV-light and blue light

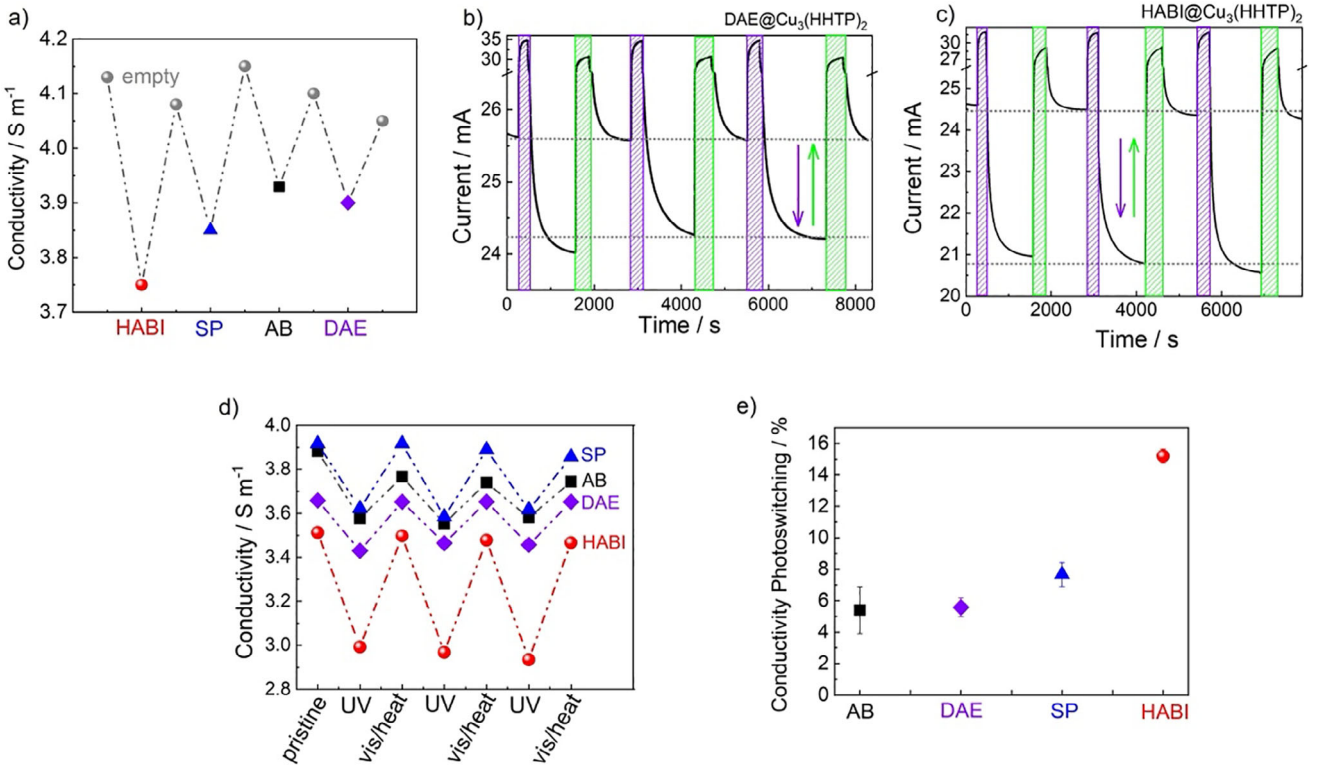

Figure 3. a) Conductivity of one $Cu_3(HHTP)_2$ SURMOF sample before and after loading and unloading with AB, DAE, SP and HABI. b) and c) The current versus time during three consecutive switching cycles of the DAE@$Cu_3(HHTP)_2$ and HABI@$Cu_3(HHTP)_2$ samples at +1 V. The violet boxes represent UV light irradiation and the green boxes represent visible light irradiation or thermal relaxation. Please note the essentially instant current increases during the light irradiation (at the colored boxes) are caused by the photoconduction in the MOF and not by the photoisomerization of the guests in the pores. The Y-scale changes at 26.5mA b) and 25.5 mA c), allowing better visibility of the current values in the dark (i.e., without light irradiation). The plots without changes in the axis are shown in Figure S6 (Supporting Information). d) The conduction changes during three consecutive switching cycles of the $Cu_3(HHTP)_2$ SURMOF loaded with AB, DAE, SP, and HABI, see labels. e) Conductivity changes of the four photoswitches in the $Cu_3(HHTP)_2$ SURMOF film caused by UV irradiation. The reference value is the conductivity of the photoswitch@$Cu_3(HHTP)_2$ sample with the photoswitch in the thermodynamically stable state (*trans* AB, open-ring DAE, SP, and dimer HABI).

results in a reversible switching of the current between 27.2 to 25.1 mA.

The conductivities of the photoswitch@$Cu_3(HHTP)_2$ samples during 3 photoswitching cycles are shown in Figure 3d. The average conductivity changes for AB@$Cu_3(HHTP)_2$, DAE@$Cu_3(HHTP)_2$, SP@$Cu_3(HHTP)_2$ and HABI@$Cu_3(HHTP)_2$ are found to be 5.4 ± 1.5%, 5.6 ± 0.6%, 7.7 ± 0.8% and 15.2 ± 0.5%, respectively, Figure 3e. (Average values with the standard deviations as errors.) Remarkable, HABI@$Cu_3(HHTP)_2$ exhibits the largest ON-OFF-photoswitching conduction ratio.

We like to stress that these conduction values are determined in the dark, this means without light irradiation. During light irradiation, this means when the UV or visible light is switched on or off, an instant current increase or decrease, respectively, can be observed. Most likely, these fast current changes are caused by photoconduction, which means by light-induced excitation of the material followed by a charge (i.e., electron-hole) separation. Such photoconduction, which only occurs under light irradiation and does not result in conductivity changes in the dark, was explored for different MOF materials[46–49] and is not studied in detail here.

For a better understanding of the conduction changes, detailed calculations of the electronic properties were performed. Although conducting MOFs (like $Cu_3(HHTP)_2$ and similar MOFs) were explored intensively in the last decade,[50,51] its conduction mechanism is not unambiguously deciphered. Many theoretical investigations indicate a metallic conductivity, which means a band-like (ballistic) charge transport with a finite density of states (DOS) at the Fermi level.[51–53] There, the conductivity of the material is proportional to the DOS at the Fermi level. To understand the different conductivities observed for the MOF film containing various molecular isomers, we focused our investigation on the azobenzene molecule in its *cis* and *trans* conformations in a monolayer $Cu_3(HHTP)_2$ MOF and their respective impacts on the DOS in proximity to the Fermi energy. **Figure** 4a illustrates the unit cell structure of $Cu_3(HHTP)_2$ concerning various wavelengths (i.e., energy levels), along with the corresponding DOS for both *cis* and *trans* conformations of the azobenzene guest molecule. To assess the modifications in the DOS of $Cu_3(HHTP)_2$ MOF with and without incorporated molecules, we initially conducted DOS calculations on the pristine MOF as a reference. We find changes in the DOS relative to the MOF without any guests, i.e., a reduction in the DOS around the

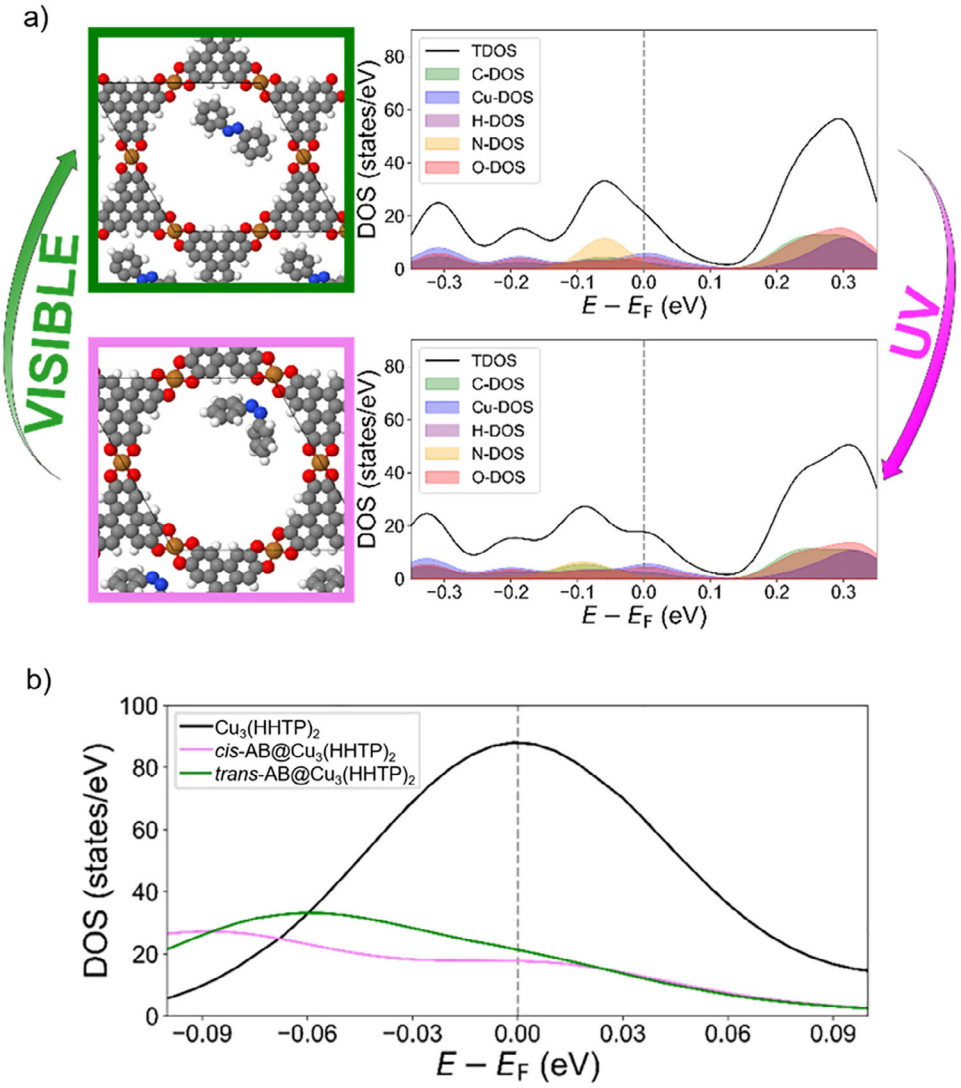

Figure 4. a) Structural illustration of the unit cell of $Cu_3(HHTP)_2$ with one azobenzene molecule in the pore (left) and the corresponding DOS (right) for *trans*-AB@$Cu_3(HHTP)_2$ (upper panel) and *cis*-AB@$Cu_3(HHTP)_2$ (lower panel). Carbon atoms are represented in gray, copper in orange, oxygen in red, nitrogen in blue, and hydrogen in white. The DOS at the respective atoms is shown, see legend, and the total DOS (TDOS). b) DOS around the Fermi level for $Cu_3(HHTP)_2$ MOF: black line, *cis*-AB@$Cu_3(HHTP)_2$: red line and *trans*-AB@$Cu_3(HHTP)_2$: purple line. The binding of azobenzene reduces the DOS peak around the Fermi level. The corresponding peak is higher for *trans*-AB compared to *cis*-AB. The conductivity of the material is proportional to the density of states at the Fermi level in a trend that agrees with those observed in experiments.

Fermi level for both guest molecule isomers. When we examine the Fermi energy, it becomes evident that the DOS for the *cis*-azobenzene guest is lower than that of the *trans*-azobenzene guest. Although these *trans*/*cis* changes are smaller than the with/without-guest changes, a clear difference of the DOS can be seen, see Figure 4. This means the DOS is modified by switching the guest between *trans* and *cis*. Given that the DOS in the structure of the guest-free MOF is populated with a higher density of charge carriers, we expect a higher conductivity (Figure 4b). The DOS in the vicinity of the Fermi energy has also been calculated for $Cu_3(HHTP)_2$ MOF incorporating DAE and SP molecules. The calculations confirm a reduction in the MOF's conductance upon UV-induced isomerization of the guest molecules (Figures S7 and S8, Supporting Information). For the HABI molecule, calculations were successfully performed for the dimer state within the MOF. However, modeling the photoinduced cleavage of HABI into two separate radical species within the MOF structure proved to be significantly more complex. This complexity arises from the need to accurately represent the spatial distribution and interactions of two distinct molecular entities within the confined pores of the MOF (Figure S9, Supporting Information).

The local DOS around the Fermi level shows the change in carriers' density regarding the embedded molecule incorporated with the $Cu_3(HHTP)_2$ MOF. It shows that the charge carrier at the Fermi level (and, thus, the conductivity which is proportional) will change regarding the conformation of the embedded molecule. This level for *cis*-AB, MC, and closed-DAE

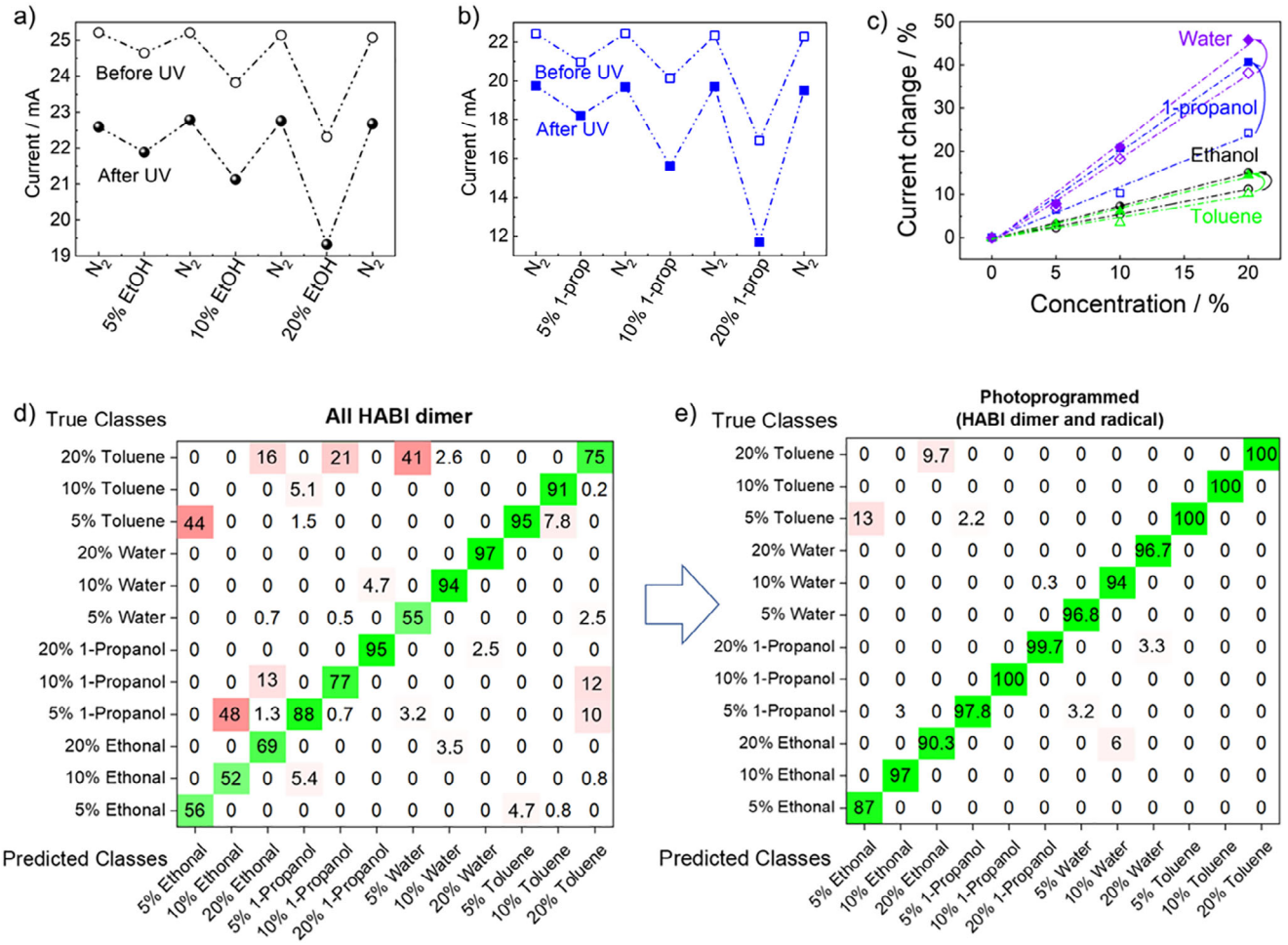

Figure 5. Sensing performance of HABI@$Cu_3(HHTP)_2$ SURMOF film. The current changes in an atmosphere of a) ethanol and b) 1-propanol with different partial pressures. The sample is in the pristine dimer-HABI state before irradiation (open symbols) and in the radical-HABI state upon UV-irradiation (solid symbols). c) The current change of HABI@$Cu_3(HHTP)_2$ pristine (open symbols) and after UV irradiation (solid symbols) versus the vapor partial pressure of different analytes, see labels. d) and e) Confusion matrix for the identification of the analyte molecules (toluene, water, 1-propanol, and ethanol) at various relative vapor pressures (5%, 10%, and 20%). The data are based on the SURMOF sensor in the HABI dimer state d) as well as on the HABI dimer and radical state e). The numbers are percentages of classifications. Correct classifications are on the diagonal (green), and misclassifications are the other values (red). The classification is determined by kNN. The average classification accuracy for all 4 VOCs and all 3 concentrations is 83.5% d) and 98.7% e).

conformation is at the lowest level. In all studied cases, the guest molecules reduced the DOS around the Fermi level, which is the reason for the reduction in conductivity. We like to stress that, although the photoswitches are only embedded in the pores and are not incorporated in the framework, the conductivity of the framework is switched indirectly by affecting the DOS of the framework.

The present study shows the proof-of-principle of photoswitching the conduction in a highly-conducting MOF. We believe the present study represents a good starting point to explore the impact of the photoswitch functionalization and loading density, the solvent for the loading, the MOF structure (e.g., $Ni_3(HHTP)_2$, or other conducting MOFs), or the temperature on the conduction switching performance.

In the following, we focus on exploring the sensor performance of the HABI@$Cu_3(HHTP)_2$ SURMOF film. To this aim, the chemiresistive properties of $Cu_3(HHTP)_2$ as a response to the exposure to different atmospheres of volatile organic compounds (VOCs) are used.[50] In this proof-of-principle study, we chose ethanol, 1-propanol, toluene, and water as probe vapors. We chose these VOC analytes due to their different sizes and due to their different polarities, since a strong impact of the polarity is expected.[54,55] We recorded the change of the current at a constant DC voltage of +1 V, **Figures 5** and S10–S11 (Supporting Information). Figure 5a,b show the response of HABI@$Cu_3(HHTP)_2$ to ethanol and propanol vapor with partial pressures of 5%, 10%, and 20%. For ethanol, while the observed current reductions were 2.3%, 5.5%, and 11.2%, respectively, for the sample in the dimer state, the corresponding current drops were 3.1%, 7.2%, and 15.1%, respectively, in the radical state, Figure 5c. This means the HABI@$Cu_3(HHTP)_2$ SURMOF film in the radical state exhibits an ethanol sensitivity enhanced by 35% compared to the dimer state. A similar enhancement of the sensitivity was also found for the other analyte molecules,

precisely, a selectivity enhancement of 63% for 1-propanol, 43% for toluene, and 16% for water. The transient current data, which means the current versus time during the analyte vapor exposure, are shown in Figure S11 (Supporting Information). It shows that the response time (which is the time for the uptake of the analyte molecules by the HABI@$Cu_3(HHTP)_2$ MOF) is in the order of a few minutes and, after the loading, the signal is rather stable. We believe the enhancement of the signal (i.e., of the conductance change for the VOC analyte exposure) of the HABI@$Cu_3(HHTP)_2$ SURMOF upon UV-irradiation is caused by the enhanced uptake amount of the VOC molecules by the sample in the radical state compared to the dimer state, as found in a previous study.[43] This enhanced uptake amount is caused by an enhanced guest affinity. Based on previous studies,[54] we believe that a major part of the changes of the affinity is caused by the changes of the polarity of the photoswitches but further, more complex effects may also contribute.

As a result of the change of the guest affinity (i.e., of the sensitivity) upon HABI photoisomerization, the sensor data can be used to identify the probe molecule. This concept was previously introduced as "photo-programmable sensors".[55] To quantitatively evaluate the sensor performance of the HABI@$Cu_3(HHTP)_2$ SURMOF film, the sensor data are classified by a k-nearest neighbor (kNN) machine learning algorithm, see supporting information. For the HABI@SURMOF sensor in the dimer state, the unambiguous identification of different guests and concentrations is difficult, Figure 5d. Here, for toluene, water, 1-propanol, and ethanol at relative vapor pressures of 5%, 10% and 20%. For example, a vapor of 5% 1-propanol is also falsely identified as 10% ethanol. As a result, the average classification accuracy is only 83.5%.

The situation changes after irradiation with UV light and using the sensor response of the HABI@$Cu_3(HHTP)_2$ SURMOF in the dimer and radical states, Figure 5e. There, all vapors at all concentrations are identified correctly and the average classification accuracy is remarkable 98.7%. This means this photoprogrammed chemiresistive sensor enables the reliable identification and discrimination of VOCs with varying partial pressures.

3. Conclusion

We present a series of highly conductive photoresponsive materials, which are made of MOF films of type $Cu_3(HHTP)_2$ with embedded photochromic molecules of type AB, DAE, SP, and HABI in the pores. The photoswitch@$Cu_3(HHTP)_2$ films possess high conductivities in the range of 3–4 S m^{-1}, that can be reversibly modulated by the loading and unloading of the photoswitches in the pores as well as by their light-induced isomerization. The largest conduction switching ratio was observed for HABI@$Cu_3(HHTP)_2$, where the conductivity was reversibly and repeatably photo-modulated by 15%. This conduction switching is explained by the calculated DOS around the Fermi level in the photoswitch@MOFs. The introduction and isomerization of guest molecules influence the DOS, thereby modifying the material's electrical conductivity. Additionally, HABI@$Cu_3(HHTP)_2$ demonstrates notable sensing properties for common VOCs, where the chemiresistive sensitivity can be enhanced by up to 60% when photoswitching the film and the selectivity is dramatically increased. This study presents the first highly conductive and photoswitchable material. Our findings underscore the significant potential of such hybrid MOF films for diverse smart materials and sensing applications.

4. Experimental Section

Materials: The chemicals, i.e., copper (II) acetate (99.9%, Alfa Aesar), 2,3,6,7,10,11-hexahydroxytriphenylene (98%, TCI), 11-mercapto-1-undecanol (99%, Sigma Aldrich), 2,2′-bis(2-chlorophenyl)-4,4′,5,5′-tetraphenyl-2′H-1,2′-biimidazole (*o*-Cl-HABI, 98%, TCI), 6-Nitro-1′,3′,3′-trimethylspiro[2H-1-benzopyran-2,2′-indolin] (nitro-SP, 98%, Sigma Aldrich), *trans*-Azobenzene (AB, Sigma Aldrich), 1,2-Bis(2-methyl-5-(pyridin-4-yl)thiophen-3-yl)cyclopent-1-ene (pyridinyl-DAE, 95%, Ambeed), toluene (99.7%, VWR chemicals), 1-propanol (99.5%, VWR chemicals) and ethanol (99.5%, VWR Chemicals), were purchased from Alfa Aesar, TCI, Sigma Aldrich and Ambeed. They were used without further purification. The substrates for the SURMOF films were quartz glass from *GVB Solutions in Glass* and glass sheets with deposited interdigitated gold electrodes with a gap width of 10 µm and a total gap length of 1.67 m from *Metrohm*.

MOF Film Synthesis and Photoswitch Embedment: $Cu_3(HHTP)_2$ SURMOFs were prepared in a layer-by-layer fashion by alternatively dipping the substrates in the solutions of the MOF components, i.e., ethanolic 0.1 mM copper(II) acetate solution and ethanolic 0.01 mM HHTP solution using a dipping robot as reported.[56] The dipping times were 10 min for the copper acetate solution and 15 min for the HHTP solution, followed by a dipping step for 2 min with pure ethanol to remove residual reactants. The samples were prepared in 200 synthesis cycles. Afterward, the samples were immersed in ethanolic 0.01 mM HHTP solution, annealed in a 60-degree oven for 20 h and the surface was cleaned with ethanol before use.[37] The SURMOF substrates were functionalized by oxygen plasma treatment.

The embedment of AB, DAE, SP and HABI photochromic molecules in the pores of the $Cu_3(HHTP)_2$ SURMOFs film was performed by soaking the MOF sample in 5mM AB, DAE, SP and HABI ethanolic solution at room temperature for 24 h, enabling the uptake by the MOF, this means the diffusion and adsorption of the photoswitches in the MOF pores. Afterward, the sample surface was briefly rinsed with ethanol and the sample was dried in a flow of pure nitrogen.

Characterizations: The X-ray diffraction (XRD) data of the MOF films were recorded with a Bruker D8 ADVANCE X-ray diffractometer with Cu-Kα radiation ($\lambda = 0.154$ nm). The SEM measurements were performed on a TESCAN VEGA3. To avoid charging effects, all samples were coated with a 3–4 nm-thick platinum film before recording the SEM images. UV–vis spectroscopy in transmission mode was explored by a Cary5000 spectrometer with an UMA unit from Agilent.

DC conductivity Measurements, Photoswitching, and Sensor Experiments: The electrical properties of the hybrid SURMOF thin film were measured using a Keithley 2635B Source-Meter. The sample was placed in a home-built chamber. For the light irradiation of the sample, LEDs with 365nm (UV), 455nm (blue), and 530 nm (green) were used. The power density at the sample surface was roughly 100 mW cm^{-2}. The duration of the light irradiation was ≈5–7min. (We refrained from longer irradiation times since it might result in irreversible reactions, in particular for photoswitches like SP.) Thermal relaxation was achieved through a 100 W heating lamp. The gas atmosphere was meticulously controlled by purging the chamber with nitrogen, allowing for enrichment with various vapor molecules. Ethanol, 1-propanol, toluene, and water vapors were generated by directing the nitrogen flow through a wash bottle (i.e., bubbler) containing the respective liquids. This method allows to achieve vapor pressures close to the saturated vapor pressure values:[57,58] toluene (4.0 kPa), ethanol (8.0 kPa), 1-propanol (2.0 kPa) and water (3.2 kPa) at room temperature (295 K). For the generation of analyte vapor with reduced concentrations (e.g., 10%, 20%, etc.), a mixture was prepared by combining a pure nitrogen flow with a nitrogen flow enriched with the vapor in various ratios.

Sensor Data Analysis: Data analysis and classification were performed using standard k-nearest neighbor (k-NN) algorithms via a program code

written in *Python 3* and performed in the open-source platform: Jupyter Notebook. For the k-NN, a total of 23 400 data points for all 4 VOC molecules in 3 different partial pressures were collected. The K value in k-NN was set to 150 (which is close to the square root of 23 400). The data were classified using 5-fold cross-validation, where 70% of the data points were used as the training set, and 30% were used as the test set. The outcome of the k-NN algorithm is the grouping of the data into the different classes and the comparison of the assignments to the classes that were correct or wrong, as shown in the confusion matrix. The used program code is given in SI, see also refs. [59,60].

DOS Calculation: The fully relaxed structure of $Cu_3(HHTP)_2$ MOF was obtained by the density functional theory (DFT) calculations using the Vienna Ab-initio Simulation Package (VASP).[61] The Perdew-Burke-Ernzerhof (PBE) functional and the projector augmented wave (PAW) method[62] were used for calculations. The cutoff energy of plane waves was set to 500 eV. The k-point mesh was set to $2 \times 2 \times 1$ and for DOS was set to $3 \times 3 \times 2$. The structures were relaxed until the forces on the atoms were less than 0.02 eV A^{-1}. The many-body dispersion energy with fractionally ionic model for polarizability was used to include the dispersion correction.[63] The DOS were calculated using the charge density of one single point calculation for the combined system. For the structure visualization, *Jmol* is used in single-unit cell representation (Available: http://jmol.sourceforge.net/).

Supporting Information

Supporting Information is available from the Wiley Online Library or from the author.

Acknowledgements

This research was funded by the Deutsche Forschungsgemeinschaft (DFG) via SPP 1928 COORNETs (HE7036/6 and WE1863/37) and under Germany's Excellence Strategy for the Excellence Cluster "3D Matter Made to Order" (Grant No. EXC2082/1390761711) and by the Carl Zeiss Foundation. This work was performed on the HoreKa supercomputer funded by the Ministry of Science, Research and the Arts Baden-Württemberg and by the Federal Ministry of Education and Research and bwHPC JUSTUS 2 funded by the state of Baden-Württemberg. Funded by the European Union (ERC, DYONCON, 101043676). Views and opinions expressed are, however those of the author(s) only and do not necessarily reflect those of the European Union or the European Research Council. Neither the European Union nor the granting authority can be held responsible for them. YL also thanks the China Scholarship Council (CSC) for financial support.

Conflict of Interest

The authors declare no conflict of interest.

Data Availability Statement

The data that support the findings of this study are available on ZENODO repository under https://doi.org/10.5281/zenodo.15000551.

Keywords

conductivity, metal–organic frameworks, photoswitching, sensors

Received: December 1, 2024
Revised: February 19, 2025
Published online:

[1] *Molecular Switches* (Eds: B. L. Feringa, W. R. Browne), Wiley, Hoboken, New Jersey **2011**.
[2] F. D. Jochum, P. Theato, *Chem. Soc. Rev.* **2013**, *42*, 7468.
[3] Z. L. Pianowski, *Chemistry-a European Journal* **2019**, *25*, 5128.
[4] M. Irie, et al., *Chem. Rev.* **2014**, *114*, 12174.
[5] H. M. D. Bandara, S. C. Burdette, *Chem. Soc. Rev.* **2012**, *41*, 1809.
[6] T. Kawai, Y. Nakashima, M. Irie, *Adv. Mater.* **2005**, *17*, 309.
[7] M E. McConney, M. Rumi, N P. Godman, U N. Tohgha, T J. Bunning, *Adv. Opt. Mater.* **2019**, *7*, 1900429.
[8] L. Kortekaas, W. R. Browne, *Chem. Soc. Rev.* **2019**, *48*, 3406.
[9] T. Kawai, T. Kunitake, M. Irie, *Chem. Lett.* **1999**, *28*, 905.
[10] V. Schneider, T. Strunskus, M. Elbahri, F. Faupel, *Carbon* **2015**, *90*, 94.
[11] S. Kitagawa, *Chem. Soc. Rev.* **2014**, *43*, 5415.
[12] H. C. Zhou, J. R. Long, O. M. Yaghi, *Chem. Rev.* **2012**, *112*, 673.
[13] W. H. Li, et al., *EnergyChem* **2020**, *2*, 100029.
[14] C. Chakravarty, B. Mandal, P. Sarkar, *J. Phys. Chem. C* **2016**, *120*, 28307.
[15] D. Sheberla, J C. Bachman, J S. Elias, C. J. Sun, Y. Shao-Horn, M. Dinca, *Nat. Mater.* **2017**, *16*, 220.
[16] V. Stavila, A. A. Talin, M. D. Allendorf, *Chem. Soc. Rev.* **2014**, *43*, 5994.
[17] M. Hmadeh, Z. Lu, Z. Liu, F. Gándara, H. Furukawa, S. Wan, V. Augustyn, R. Chang, L. Liao, F. Zhou, E. Perre, V. Ozolins, K. Suenaga, X. Duan, B. Dunn, Y. Yamamto, O. Terasaki, O M. Yaghi, *Chem. Mater.* **2012**, *24*, 3511.
[18] L. De, M. Gonzalez-Juarez, et al., *J. Mater. Chem. A* **2020**, *8*, 13197.
[19] A. Mähringer, A C. Jakowetz, J M. Rotter, B J. Bohn, J K. Stolarczyk, J. Feldmann, T. Bein, D D. Medina, *ACS Nano* **2019**, *13*, 6711.
[20] V. Rubio-Gimenez, et al., *Adv. Mater.* **2018**, *30*, 1704291.
[21] H. A. Schwartz, U. Ruschewitz, L. Heinke, *Photochem. Photobiol. Sci.* **2018**, *17*, 864.
[22] F. Bigdeli, C T. Lollar, A. Morsali, H. C. Zhou, *Angew. Chem.* **2020**, *59*, 4652.
[23] R. Haldar, L. Heinke, C. Wöll, *Adv. Mater.* **2020**, *32*, 30.
[24] Y. Z. Jiang, L. Heinke, *Langmuir* **2021**, *37*, 2.
[25] A. B. Kanj, K. Müller, L. Heinke, *Macromol. Rapid Commun.* **2017**, *38*, 1700239.
[26] J. Park, D. Yuan, K T. Pham, J. R. Li, A. Yakovenko, H. C. Zhou, *J. Am. Chem. Soc.* **2012**, *134*, 99.
[27] A. Schaate, S. Dühnen, G. Platz, S. Lilienthal, A M. Schneider, P. Behrens, *Eur. J. Inorg. Chem.* **2012**, *2012*, 790.
[28] Y. Jiang, et al., *Angew. Chem., Int. Ed.* **2023**, e202218052.
[29] I M. Walton, J M. Cox, J A. Coppin, C M. Linderman, D G. (D) Patel, J B. Benedict, *Chem. Commun.* **2013**, *49*, 8012.
[30] A. B. Kanj, A. Chandresh, A. Gerwien, S. Grosjean, S. Bräse, Y. Wang, H. Dube, L. Heinke, *Chem. Sci.* **2020**, *11*, 1404.
[31] F. Zhang, X. Zou, W. Feng, X. Zhao, X. Jing, F. Sun, H. Ren, G. Zhu, *J. Mater. Chem.* **2012**, *22*, 25019.
[32] C R. Martin, K. C. Park, G A. Leith, J. Yu, A. Mathur, G R. Wilson, G B. Gange, E L. Barth, R T. Ly, O M. Manley, K L. Forrester, S G. Karakalos, M D. Smith, T M. Makris, A K. Vannucci, D V. Peryshkov, N B. Shustova, *J. Am. Chem. Soc.* **2022**, *144*, 4457.
[33] Y. Liu, Y. Jiang, L. Heinke, *Langmuir* **2023**, *40*, 474.
[34] S. Garg, H. Schwartz, M. Kozlowska, A. B. Kanj, K. Müller, W. Wenzel, U. Ruschewitz, L. Heinke, *Angew. Chem., Int. Ed.* **2019**, *58*, 1193.
[35] M. Mostaghimi, H. Pacheco Hernandez, Y. Jiang, W. Wenzel, L. Heinke, M. Kozlowska, *Commun. Chem.* **2023**, *6*, 275.
[36] O. Shekhah, H. Wang, S. Kowarik, F. Schreiber, M. Paulus, M. Tolan, C. Sternemann, F. Evers, D. Zacher, R A. Fischer, C. Wöll, *J. Am. Chem. Soc.* **2007**, *129*, 15118.
[37] M. S. Yao, X. J. Lv, Z. H. Fu, W. H. Li, W. H. Deng, G. D. Wu, G. Xu, *Angewandte Chemie-International Edition* **2017**, *56*, 16510.
[38] Z. G. Gu, A. Pfriem, S. Hamsch, H. Breitwieser, J. Wohlgemuth, L. Heinke, H. Gliemann, C. Wöll, *Microporous Mesoporous Mater.* **2015**, *211*, 82.

[39] D T. Valley, M. Onstott, S. Malyk, A V. Benderskii, *Langmuir* **2013**, *29*, 11623.
[40] A. Gonzalez, E. S. Kengmana, M. V. Fonseca, G. G. D. Han, *Mater. Today Adv.* **2020**, *6*, 100058.
[41] A. Knebel, L. Sundermann, A. Mohmeyer, I. Strauß, S. Friebe, P. Behrens, J. Caro, *Chem. Mater.* **2017**, *29*, 3111.
[42] K. Müller, J. Wadhwa, J. Singh Malhi, L. Schöttner, A. Welle, H. Schwartz, D. Hermann, U. Ruschewitz, L. Heinke, *Chem. Commun.* **2017**, *53*, 8070.
[43] Y. D. Liu, Y. Z. Jiang, L. Heinke, *Langmuir* **2023**, *40*, 474.
[44] Y. Liu, Y. Yang, D. Shi, M. Xiao, L. Jiang, J. Tian, G. Zhang, Z. Liu, X. Zhang, D. Zhang, *Adv. Mater.* **2019**, *31*, 1902576.
[45] J. M. Wrogemann, M. J. Lüther, P. Bärmann, M. Lounasvuori, A. Javed, M. Tiemann, R. Golnak, J. Xiao, T. Petit, T. Placke, M. Winter, *Angew. Chem., Int. Ed. Engl.* **2023**, *62*, 202303111.
[46] D. Wang, S. Ostresh, D. Streater, P. He, J. Nyakuchena, Q. Ma, X. Zhang, J. Neu, G W. Brudvig, J. Huang, *Angew. Chem., Int. Ed.* **2023**, *62*, 202309505.
[47] C. Li, H. Schopmans, L. Langer, S. Marschner, A. Chandresh, J. Bürck, Y. Tsuchiya, A. Chihaya, W. Wenzel, S. Bräse, M. Kozlowska, L. Heinke, *Angew. Chem., Int. Ed.* **2023**, *62*, 202217377.
[48] X. Liu, M. Kozlowska, T. Okkali, D. Wagner, T. Higashino, G. Brenner-Weiß, S M. Marschner, Z. Fu, Q. Zhang, H. Imahori, S. Bräse, W. Wenzel, C. Wöll, L. Heinke, *Angew. Chem., Int. Ed.* **2019**, *58*, 9590.
[49] J. B. Zhang, Yi-Bo Tian, Z. G. Gu, J. Zhang, *Nano-Micro Lett.* **2024**, *16*, 253.
[50] M G. Campbell, S F. Liu, T M. Swager, M. Dinca, *J. Am. Chem. Soc.* **2015**, *137*, 13780.
[51] M. Wang, R. Dong, X. Feng, *Chem. Soc. Rev.* **2021**, *50*, 2764.
[52] G. Skorupskii, et al., *Proc. Natl. Acad. Sci. USA* **2022**, *119*, 2205127119.
[53] P. H. Souza, W. Orellana, *J. Phys. Chem. C* **2025**, *129*, 3285.
[54] Z. Wang, S. Grosjean, S. Bräse, L. Heinke, *ChemPhysChem* **2015**, *16*, 3779.
[55] P. Qin, S. Okur, C. Li, A. Chandresh, D. Mutruc, S. Hecht, L. Heinke, *Chem. Sci.* **2021**, *12*, 15700.
[56] Z. G. Gu, A. Pfriem, S. Hamsch, H. Breitwieser, J. Wohlgemuth, L. Heinke, H. Gliemann, C. Wöll, *Microporous Mesoporous Mater.* **2015**, *211*, 82.
[57] P. Qin, S. Okur, C. Li, A. Chandresh, D. Mutruc, S. Hecht, L. Heinke, *Chem. Sci.* **2021**, *12*, 15700.
[58] C. Li, Z. Zhang, L. Heinke, *Phys. Chem. Chem. Phys.* **2022**, *24*, 3994.
[59] K. Zhan, Y. Z. Jiang, L. Heinke, *Chem. Commun.* **2023**, *59*, 8704.
[60] K. Zhan, et al., *Adv. Mater. Interfaces* **2023**, *10*, 2300329.
[61] G. Kresse, J. Furthmüller, *Comput. Mater. Sci.* **1996**, *6*, 15.
[62] J. P. Perdew, K. Burke, M. Ernzerhof, *Phys. Rev. Lett.* **1996**, *77*, 3865.
[63] T. Bučko, S. Lebègue, T. Gould, J. G. Ángyán, *J. Phys.:Condens. Matter* **2016**, *28*, 045201.